ARMY RESEARCH LABORATORY

Delivery of Modular Lethality via a Parent–Child Concept

by Frank Fresconi and Müge Fermen-Coker

ARL-TR-7191 **February 2015**

NOTICES

Disclaimers

The findings in this report are not to be construed as an official Department of the Army position unless so designated by other authorized documents.

Citation of manufacturer's or trade names does not constitute an official endorsement or approval of the use thereof.

Destroy this report when it is no longer needed. Do not return it to the originator.

Army Research Laboratory
Aberdeen Proving Ground, MD 21005-5066

ARL-TR-7191 **February 2015**

Delivery of Modular Lethality via a Parent–Child Concept

Frank Fresconi and Müge Fermen-Coker
Weapons and Materials Research Directorate, ARL

REPORT DOCUMENTATION PAGE			Form Approved OMB No. 0704-0188

1. REPORT DATE *(DD-MM-YYYY)*	2. REPORT TYPE	3. DATES COVERED (From - To)
February 2015	Final	1 October 2013–30 September 2014

4. TITLE AND SUBTITLE	5a. CONTRACT NUMBER
Delivery of Modular Lethality via a Parent–Child Concept	5b. GRANT NUMBER
	5c. PROGRAM ELEMENT NUMBER

6. AUTHOR(S)	5d. PROJECT NUMBER
Frank Fresconi and Müge Fermen-Coker	AH80
	5e. TASK NUMBER
	5f. WORK UNIT NUMBER

7. PERFORMING ORGANIZATION NAME(S) AND ADDRESS(ES)	8. PERFORMING ORGANIZATION REPORT NUMBER
US Army Research Laboratory ATTN: RDRL-WML-E Aberdeen Proving Ground, MD 21005-5066	ARL-TR-7191

9. SPONSORING/MONITORING AGENCY NAME(S) AND ADDRESS(ES)	10. SPONSOR/MONITOR'S ACRONYM(S)
	11. SPONSOR/MONITOR'S REPORT NUMBER(S)

12. DISTRIBUTION/AVAILABILITY STATEMENT

Approved for public release; distribution is unlimited.

13. SUPPLEMENTARY NOTES

14. ABSTRACT

Optimal lethal efficiency may be achieved by delivering small modules with desired patterns against complex targets. The focus of this study is reliable production of prescribed impact locations of multiple small flight bodies at low cost. A parent–child concept based on reduced feedback and simple control mechanisms is introduced to achieve this goal. Guidance and flight-control algorithms are derived for this concept using flight dynamics and optimization theory. High-fidelity flight models are used to prove the concepts and techniques. Results from simulations coupling multiple bodies in flight demonstrate successful delivery of child bodies to desired locations despite significant nonlinearities and system uncertainties.

15. SUBJECT TERMS

modular lethality, guidance, flight

16. SECURITY CLASSIFICATION OF:			17. LIMITATION OF ABSTRACT	18. NUMBER OF PAGES	19a. NAME OF RESPONSIBLE PERSON
a. REPORT	b. ABSTRACT	c. THIS PAGE			Frank Fresconi
Unclassified	Unclassified	Unclassified	UU	31	19b. TELEPHONE NUMBER (*Include area code*) (410) 306-0794

Standard Form 298 (Rev. 8/98)
Prescribed by ANSI Std. Z39.18

Contents

List of Figures

Acknowledgments

The authors gratefully acknowledge the contributions of Ilmars Celmins for solid modeling, Sidra Silton for computational fluid-dynamics predictions, and Luke Strohm for discussions of the modular lethality concept.

INTENTIONALLY LEFT BLANK.

1. Introduction

The motivation for this study is to arbitrarily deliver lethal modules to prescribed locations on the battlefield. The basic idea is that the most efficient usage of energetic material may be achieved through precise arrangement of smaller payloads at the target site. The launch and lethal mechanism are not explicitly considered in the present work.

The means of flying these small, lethal payloads from the launcher to the target is addressed in this study. Of particular interest are concepts that reliably produce desired terminal patterns at low cost. Feedback control, whereby commands to control the system are based on feedback measurements, is a classic way to ensure high performance in a complex environment such as a battlefield. Indeed, military applications have driven guidance, navigation, and control (GNC) technologies for aircraft[1] and missiles.[2–5] Flocking or swarming behaviors of unmanned aircraft systems,[6–7] parafoils,[8] and spacecraft[9] have been investigated. Bennet et al.[6] developed a safety-critical guidance algorithm based on potential fields to fly aerial robot swarms without actuator saturation. Collision-avoidance and formation-flight algorithms for airdrop of supplies from multiple units deployed in the same airspace have been derived and verified in simulation and experiment.[8]

Guided projectile technologies have demonstrated[10–12] substantial progress recently. The emergence and subsequent gun hardening of Global Positioning System (GPS) technology has enabled precision artillery weapons.[10] Fresconi[11] used GPS feedback in a nonlinear model predictive control strategy to reduce the actuator and sensor burden on a rolling artillery and mortar projectile. Enhanced maneuverability while maintaining low-cost actuation components has been established more recently.[12] These efforts have largely focused on a single flight for larger caliber and indirect-fire applications.

The novel contributions of the present work include formulation of a unique modular-delivery concept and derivation of guidance and flight-control algorithms for this concept. A parent–child delivery strategy is introduced to meet performance goals at low cost. A flight-dynamics-based control algorithm is derived and optimization theory is applied for the guidance law. Models of the control mechanism, flight, and feedback measurements are outlined. These models are implemented in simulation with the appropriate input data along with the guidance and flight-control algorithms. Results illustrate the feasibility and key features of the novel modular-delivery concept and guidance and flight-control techniques.

2. Concept

Options for the launch of the modular-delivery concept include burst-fire or a drop from an unmanned aerial system. Regardless of the specific launch mechanism, this work assumes that multiple bodies are flying simultaneously in a relatively close proximity. The idea of a parent–child relationship is used to achieve performance metrics with simplified components. In this paradigm, a parent flight body features higher performance components (e.g., more feedback sensors, higher precision actuators, faster processors) which are exercised to accurately fly to the complex target and gather information useful for the child flight bodies. The children are shed from the parent body as appropriate, depending on the mission, and are equipped with simpler components (e.g., reduced sensor suite, minimal actuation). This notion exercises swarming behaviors to enable efficient delivery of simple, modular bodies to desired arbitrary locations against complex targets.

Consider Fig. 1 as an example. In this illustration a parent body contains image-based navigational technology and electromechanically actuated canards. Image-based navigation provides extremely accurate targeting for the parent body and also low latency information regarding optimal patterns for child bodies against complex target arrays. The electromechanical-actuation technology allows for the high maneuverability necessary for gliding, loitering, or intercepting moving and defilade targets. The benefits of these components are often offset by added cost and complexity. As a means of producing arbitrary terminal patterns without exorbitant cost, the child bodies in Fig. 1 feature a simple ranging device, such as a radar unit, and a ring of jet thrusters. As the body rolls, the ranging device permits the relative spacing to surrounding bodies to be assessed. Thruster commands can then be issued depending on the desired pattern of parent and child bodies. Communication between bodies (e.g., sensor fusion, tasking of children by parent) may also enhance performance. Trajectories flown to a complex target array using this parent–child concept are shown in the plot on the right of Fig. 1.

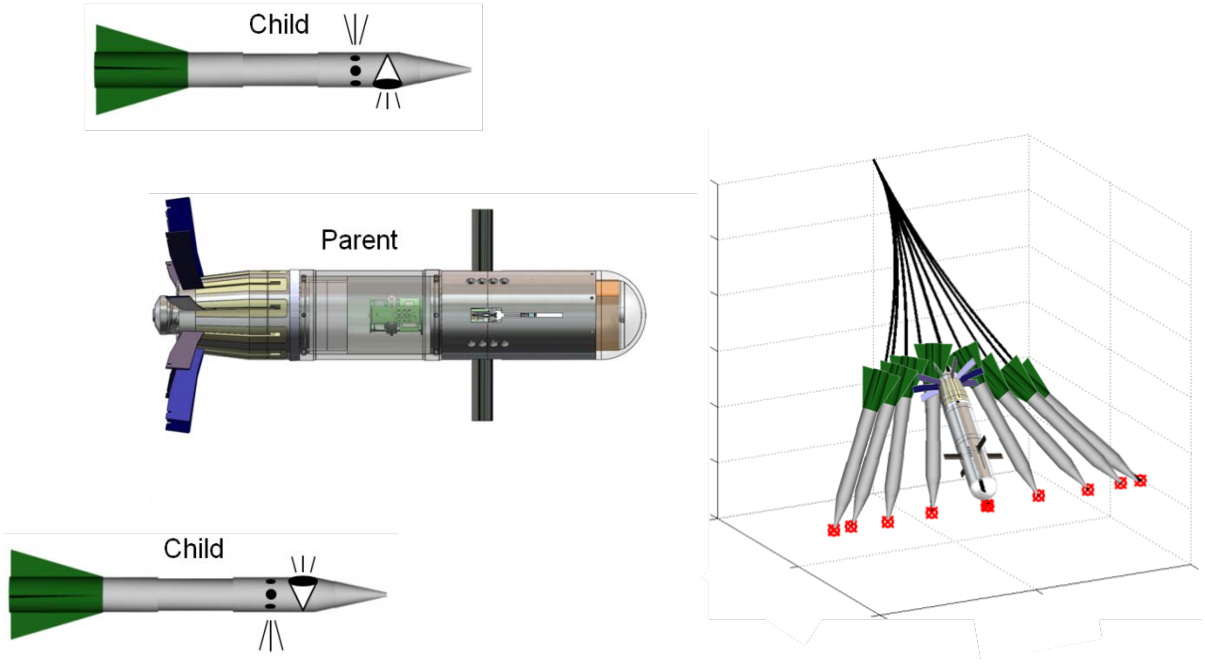

Fig. 1 Illustration of parent–child modular-delivery concept

3. Flight Models

Flight behaviors of parent and child bodies were calculated using a 6-degree-of-freedom model. Theoretical details of the body-fixed model are provided in Murphy[13] and Fresconi et al.[14] Translational and rotational kinematics given in Eq. 1 and 2 relate quantities in body-fixed coordinates ($[u \quad v \quad w]$ and $[p \quad q \quad r]$) to inertial coordinates ($[\dot{x} \quad \dot{y} \quad \dot{z}]$ and $[\dot{\phi} \quad \dot{\theta} \quad \dot{\psi}]$) through the use of the Euler angles ($[\phi \quad \theta \quad \psi]$)):

$$\begin{bmatrix} \dot{x} \\ \dot{y} \\ \dot{z} \end{bmatrix} = \begin{bmatrix} c_\theta c_\psi & s_\phi s_\theta c_\psi - c_\phi s_\psi & c_\phi s_\theta c_\psi + s_\phi s_\psi \\ c_\theta s_\psi & s_\phi s_\theta s_\psi + c_\phi c_\psi & c_\phi s_\theta s_\psi + s_\phi s_\psi \\ -s_\theta & s_\phi c_\theta & c_\phi c_\theta \end{bmatrix} \begin{bmatrix} u \\ v \\ w \end{bmatrix} \tag{1}$$

and

$$\begin{bmatrix} \dot{\phi} \\ \dot{\theta} \\ \dot{\psi} \end{bmatrix} = \begin{bmatrix} 1 & s_\phi t_\theta & c_\phi t_\theta \\ 0 & c_\phi & -s_\phi \\ 0 & s_\phi / c_\theta & c_\phi / c_\theta \end{bmatrix} \begin{bmatrix} p \\ q \\ r \end{bmatrix} . \tag{2}$$

The translational and rotational dynamics presented in Eq. 3 and 4 determine the accelerations ($[\dot{u} \quad \dot{v} \quad \dot{w}]$ and $[\dot{p} \quad \dot{q} \quad \dot{r}]$) in the body-fixed coordinate system. The mass properties (mass m, moment of inertia tensor $\vec{I}$) of the flight body are required along with the aerodynamic forces and

moments. The aerodynamic model relating states of the airframe (e.g., Mach number, angle of attack) to aerodynamic coefficient data (based on computational fluid-dynamics predictions from Silton et al.[15]) and ultimately forces and moments is not provided here.[14] Gravity is also used to determine the overall forces and moments acting on each flight body ($[X \quad Y \quad Z]$ and $[L \quad M \quad N]$):

$$\begin{bmatrix} \dot{u} \\ \dot{v} \\ \dot{w} \end{bmatrix} = \frac{1}{m}\begin{bmatrix} X \\ Y \\ Z \end{bmatrix} - \begin{bmatrix} 0 & -r & q \\ r & 0 & -p \\ -q & p & 0 \end{bmatrix}\begin{bmatrix} u \\ v \\ w \end{bmatrix} \tag{3}$$

and

$$\begin{bmatrix} \dot{p} \\ \dot{q} \\ \dot{r} \end{bmatrix} = \vec{I}^{-1}\begin{bmatrix} L \\ M \\ N \end{bmatrix} - \vec{I}^{-1}\begin{bmatrix} 0 & -r & q \\ r & 0 & -p \\ -q & p & 0 \end{bmatrix}\vec{I}\begin{bmatrix} p \\ q \\ r \end{bmatrix} \quad . \tag{4}$$

The control forces and moments for the child body are supplied by a continuously variable lateral-thruster array. These devices use some means (not addressed in this study) to smoothly throttle the thrust produced normal to the spin axis of the flight body (i.e., no control of axial component). This study assumes that thrust is always available. Aerodynamic canard control with a first-order model for actuator dynamics is used for the parent body.[14]

The feedback measurements from a ranging device on the rolling child body provide the location of all other bodies in the body-fixed coordinate system of that specific child. The 3-dimensional position of the j^{th} body with respect to the i^{th} body in the i^{th} body-fixed coordinates can be determined in the 6-degree-of-freedom model by manipulating the inertial positions of both bodies and the Euler angles of the i^{th} body according to Eq. 5. The parent uses a seeker and inertial-measurement unit[14] for feedback purposes:

$$\begin{bmatrix} x_{ij}^{B_i} \\ y_{ij}^{B_i} \\ z_{ij}^{B_i} \end{bmatrix} = \begin{bmatrix} c_\theta c_\psi & c_\theta s_\psi & -s_\theta \\ s_\phi s_\theta c_\psi - c_\phi s_\psi & s_\phi s_\theta s_\psi + c_\phi c_\psi & s_\phi c_\theta \\ c_\phi s_\theta c_\psi + s_\phi s_\psi & c_\phi s_\theta s_\psi + s_\phi s_\psi & c_\phi c_\theta \end{bmatrix}\begin{bmatrix} x_j^I - x_i^I \\ y_j^I - y_i^I \\ z_j^I - z_i^I \end{bmatrix} \quad . \tag{5}$$

The 1962 International Standard Atmosphere model provided atmospheric density and sound speed. Winds were modeled with a constant magnitude and direction. These models were implemented in simulation and integrated using a fourth-order Runge–Kutta method. Monte Carlo capability was included in the simulation such that variation or uncertainty in aerodynamics, mass properties, atmospheric, actuators, feedback measurements, and launch conditions were modeled. Finally, the simulation environment was made extensible to an arbitrary number of projectiles in flight to account for the instantaneous coupled effects of swarming flight.

4. Guidance and Flight-Control Laws

Algorithms for guiding the parent were presented in Fresconi et al.[14] Here, the focus is on guidance of the child. The relationship between feedback-measurement output and control-mechanism input is critical to flight-control law formulation. For this reason we need to relate the relative position from the ranging device to the thruster force. Fortunately, Guidos and Cooper[16] have provided such an expression. This study considered the flight response to lateral impulses similar to that proposed in the present work. The equations of motion governing flight (Eq. 1–4) were simplified for this situation and a closed-form solution was obtained. A version of this solution is shown in Eq. 6:

$$r = -\frac{C_{N_\alpha}}{C_{m_\alpha}} \frac{D}{m\bar{V}^2} \frac{(x_{TGT} - \bar{V}t)}{D} \frac{d_F}{D} F \quad . \qquad (6)$$

In this expression, r is the lateral displacement, C_{N_α} is the aerodynamic normal-force slope coefficient, C_{m_α} is the aerodynamic pitching-moment slope coefficient, D is the body diameter, m is the body mass, $\bar{V}$ is the average velocity, x_{TGT} is the downrange distance to the target, t is the time of flight, d_F is the distance of the thruster force from the body center of gravity, and F is the thruster force. Thus, Eq. 6 defines the lateral displacement (r) of a body flying toward a target with certain characteristics (C_{N_α}, C_{m_α}, D, m, $\bar{V}$, x_{TGT}, t) due to a given impulsive-control moment ($d_F F$).

This modular-delivery concept seeks prescribed distributions of child bodies around the parent. Using Eq. 6, a predictive control strategy can be built around control-force inputs based on the error between measured and desired lateral displacements. Mass properties, aerodynamics, thruster locations, and target distance can be obtained prior to launch, and average velocity and time of flight can be estimated or measured in flight. These values can be collected in a term, A_F, and the 2 components of lateral-control force can be related to the relative position feedback as shown in Eq. 7:

$$\begin{bmatrix} y_{ij}^{B_i} \\ z_{ij}^{B_i} \end{bmatrix} = -\begin{bmatrix} A_F & 0 \\ 0 & A_F \end{bmatrix} \begin{bmatrix} F_{y_{ij}}^{B_i} \\ F_{z_{ij}}^{B_i} \end{bmatrix} \quad . \qquad (7)$$

Equation 7 provides a means to command forces on a given child using ranging data to one parent or child. The swarming behavior is more complex because a method must be devised to optimize force commands to achieve a desired pattern from multiple bodies surrounding a given child. For example, a desired geometry may be satisfied between the child and the parent but not between that child and another child. This situation is depicted in Fig. 2 for a desired circular pattern of 5 children (C_1–C_5) equally spaced around the parent (P).

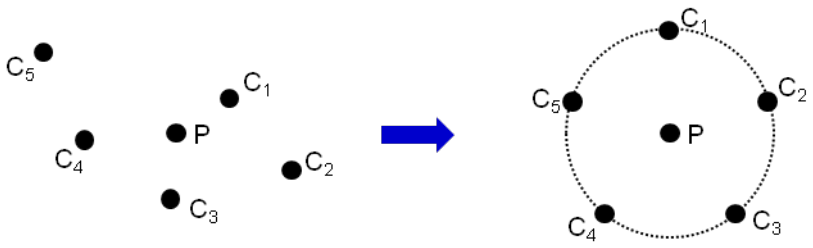

Fig. 2 Resolution of desired delivery formation for multiple bodies in flight

Optimization theory can balance the desired flight formation with the control authority available. These problems are typically cast in terms of a cost function, J:

$$J = \vec{\epsilon}^T \vec{Q} \vec{\epsilon} + \vec{u}^T \vec{R} \vec{u} \quad . \tag{8}$$

Here, the control error is $\vec{\epsilon}$ and the control action is $\vec{u}$. Weighting matrices for the control error ($\vec{Q}$) and control action ($\vec{R}$) permit tuning for desired flight-formation performance without prohibitively high control commands.

Next, the cost function is minimized with respect to the control for a specific formulation and solved to obtain an expression for the control:

$$\min J = \frac{\partial J}{\partial \vec{u}} = 0 \quad . \tag{9}$$

For the present problem we consider only the control-error portion of the cost function shown in Eq. 8 (i.e., $\vec{R} = \vec{0}$). A cost-function variable ($\vec{\epsilon}_i$), comprising the difference between the lateral-displacement feedback ($\vec{y}_i$) and the model prediction of lateral displacement from Eq. 6 ($\vec{C}\vec{u}_i$), was defined to solve this optimization problem for the i^{th} child with N total bodies:

$$\vec{\epsilon}_i = \begin{bmatrix} y_{i1}^{B_i} \\ z_{i1}^{B_i} \\ y_{i2}^{B_i} \\ z_{i2}^{B_i} \\ \vdots \\ y_{iN-1}^{B_i} \\ z_{iN-1}^{B_i} \end{bmatrix} + \begin{bmatrix} A_F & 0 & 0 & 0 & 0 & 0 & 0 \\ 0 & A_F & 0 & 0 & 0 & 0 & 0 \\ 0 & 0 & A_F & 0 & 0 & 0 & 0 \\ 0 & 0 & 0 & A_F & 0 & 0 & 0 \\ 0 & 0 & 0 & 0 & \ddots & \vdots & \vdots \\ 0 & 0 & 0 & 0 & \cdots & A_F & 0 \\ 0 & 0 & 0 & 0 & \cdots & 0 & A_F \end{bmatrix} \begin{bmatrix} F_{y_{i1}}^{B_i} \\ F_{z_{i1}}^{B_i} \\ F_{y_{i2}}^{B_i} \\ F_{z_{i2}}^{B_i} \\ \vdots \\ F_{y_{iN-1}}^{B_i} \\ F_{z_{iN-1}}^{B_i} \end{bmatrix} = \vec{y}_i + \vec{C}\vec{u}_i \quad . \tag{10}$$

Inserting Eq. 10 into Eq. 8 and 9 and manipulating yields an equation for the control of the i^{th} child as given in Eq. 11. This expression essentially follows a least-squares problem:

$$\vec{u}_i = \left(\vec{C}^T \vec{C}\right)^{-1} \vec{C}^T \vec{y}_i \quad . \quad (11)$$

The final step is to resolve the lateral commands for each body into a single command for the control-force magnitude and direction of the i^{th} child. This could be done through schemes such as weighted averaging; however, for the present work a simple average was used:

$$F_i = \frac{\sum_{j=1}^{N-1} \vec{u}_i}{N-1}$$
$$\phi_{Ci} = \tan^{-1}\left(\frac{\text{even}\sum_{j=1}^{N-1} \vec{u}_i}{\text{odd}\sum_{j=1}^{N-1} \vec{u}_i}\right) \quad . \quad (12)$$

Figure 3 depicts the manner in which control-force magnitude and direction are resolved into the body-fixed coordinate system for each child.

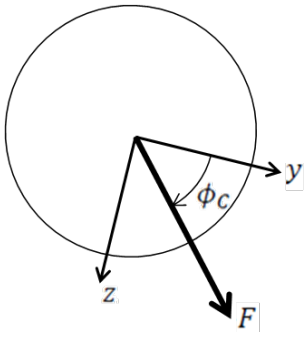

Fig. 3 Control-force magnitude and direction in body-fixed coordinates of child

5. Results

The modular-delivery concept, guidance and flight-control algorithms, and flight models were implemented in simulation for a representative 40-mm diameter, fin-stabilized airframe with thrusters located 3 calibers ahead of the center of gravity. Swarms were launched at a subsonic Mach number (150 m/s) 100 m above the ground against a target 400 m downrange. This situation may represent a launch from a small unmanned aerial system; however, the intent of this study is to demonstrate the utility of this class of technology across a wide array of applications.

Numerical experiments were conducted to assess delivery performance. In the first set of results, a parent and single child were flown under ideal conditions (e.g., no errors in feedback measurements, aerodynamics, etc.) with a desired lateral spacing of 1 m. Thus, the parent should

impact 400 m downrange and the child should range off the parent body yielding an impact 400 m downrange and 1 m off to the side.

The flight dynamics of the parent and child are provided in Fig. 4. Blue curves represent the parent and purple curves are for the child. The trajectory as a function of downrange distance is contained in the upper plots (cross range in top-left and altitude in top-right). The cross-range flight behavior shows that the parent flies along the line of fire and impacts at the target. Some oscillation appears in the child cross-range trajectory and the impact location is approximately 1 m to the side of the parent, as desired. The trajectory in the vertical plane is almost identical between the parent and child. These trajectory results suggest that this guidance and flight-control laws are successful in commanding maneuvers in the child based on ranging measurements off the parent for arbitrary modular-delivery patterns.

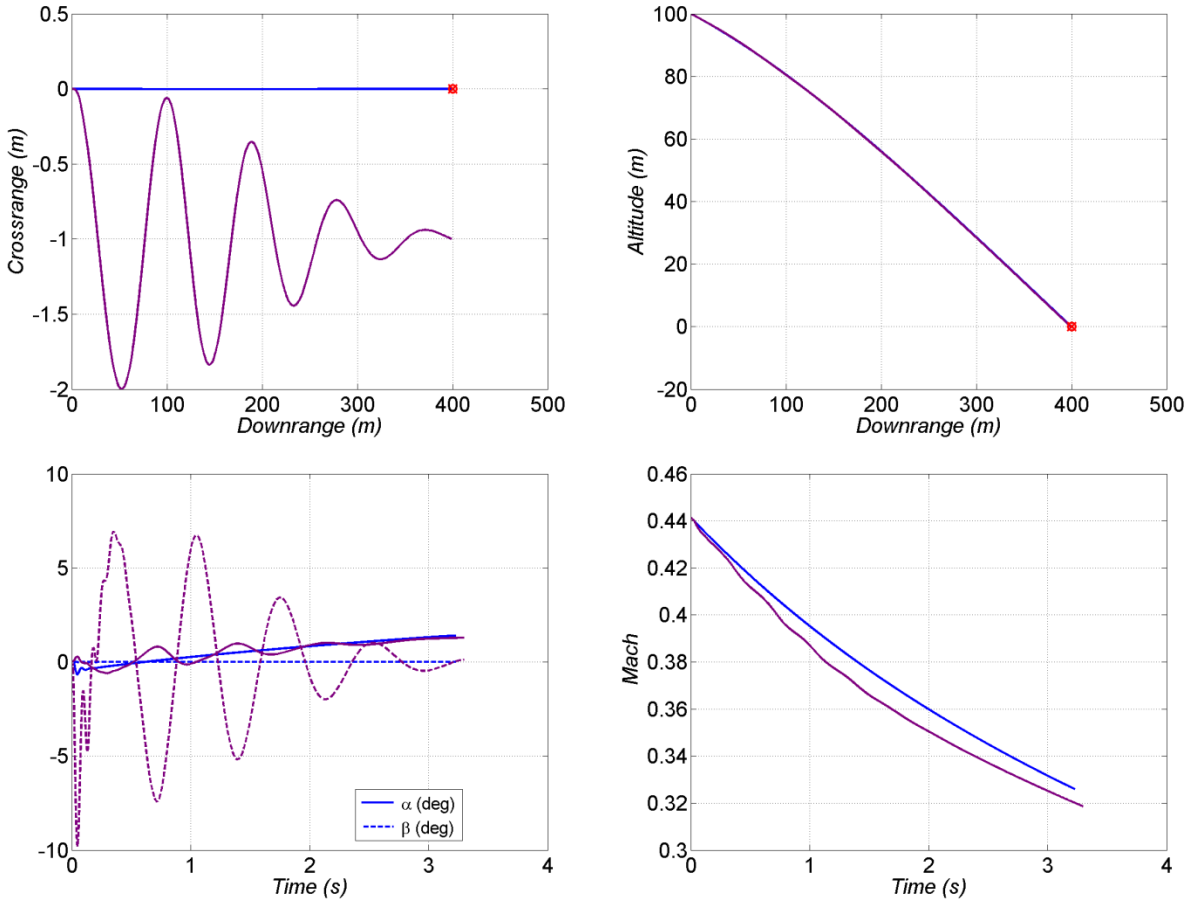

Fig. 4 Flight dynamics of parent and one child

The pitch (α, solid line) and yaw (β, dashed line) angle-of-attack histories are provided in the bottom-left plot of Fig. 4. Small total angle of attack is evident in the parent flight; there is a positive pitch angle of attack perhaps because the target is slightly beyond the ballistic range. Interestingly, the child pitch angle of attack follows the parent history with small oscillation,

which is consistent with the vertical-trajectory results. The yaw angle of attack for the child features damped oscillation (as seen in the horizontal trajectory) to some appreciable magnitudes (>5°). The Mach-number histories are shown in the bottom-right of Fig. 4. The higher total angle of attack of the child yields slightly higher velocity decay.

The control input and output for the parent with one child are provided in Fig. 5. Lateral displacements of the child from the parent obtained from the ranging device on the child are given in the left-most plot. The y-direction (solid line) mimics the horizontal trajectory as expected and demonstrates suitable control performance (1-m offset at impact). The z-direction (dashed line) data indicate small displacements as desired. These feedback measurements are used to form the control-commands input to the system. The right-most plot has dual y axes. The left y axis (blue) is for the maneuver direction (ϕ_C) and the right y axis (green) is for the maneuver magnitude (F). The child is commanded to move mainly left and right for the majority of the flight and demands some up maneuvers toward the end of the flight to keep from falling short of the parent since the child yaw–drag component was higher. The magnitude fluctuates when the child flies through nodes of the desired set point but overall is small (<2N).

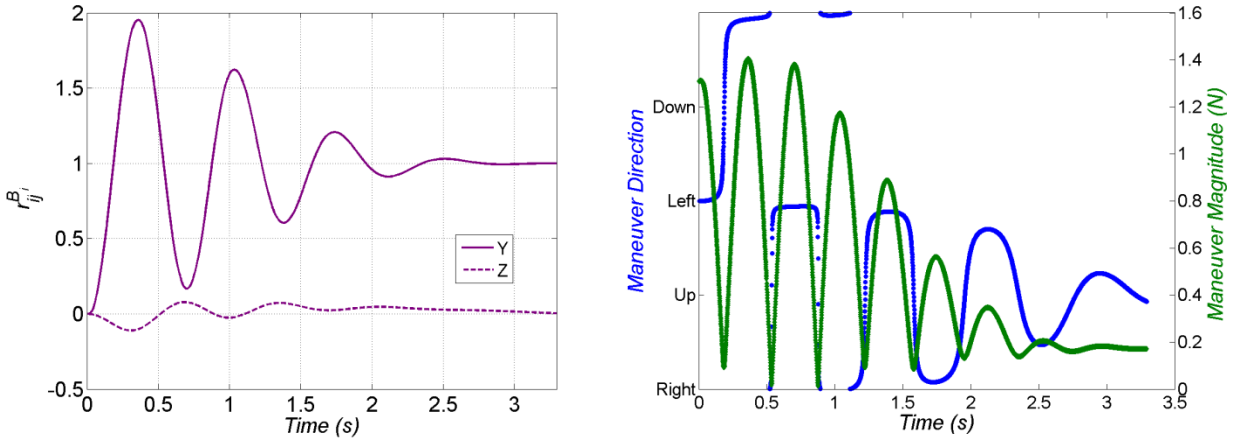

Fig. 5 Feedback output and control input of parent and one child

Some additional control metrics are detailed in Fig. 6. The upper-left plot is the time-varying control gain, A_F. These data show how a higher control demand is called for earlier in the flight regardless of the error between the feedback and model prediction. The error between the feedback and model prediction in the y and z directions is contained in the upper-right plot. Ideally, these errors would rapidly converge to zero. The data in the plot illustrate reasonable performance. Oscillation is likely due to using a position-feedback measurement with a force (or acceleration) control; essentially there is a lag between when measurements are collected and when the response appears in the system. Additionally, the guidance law is framed around the idea that we want the current lateral displacement (from the feedback) to equal the final desired lateral displacement (from the model prediction). These oscillatory effects could be removed further through a derivative or rate-feedback term in the controller or also by using an adjustable

finite horizon; for example, putting the "final" downrange distance used in the controller (Eq. 6) closer to the launcher and moving this farther toward the true target at each control update. Even without these potential enhancements the current controller performs well as evidenced by meeting the goals of the desired impact patterns. The bottom plot gives the control magnitude commands in the y and z directions that result from the error signals in the upper-right plot. As expected, larger errors in the y direction yield larger control forces. The maneuver magnitude in the right-most plot of Fig. 5 is the root–sum–square of these values in the bottom plot of Fig. 6.

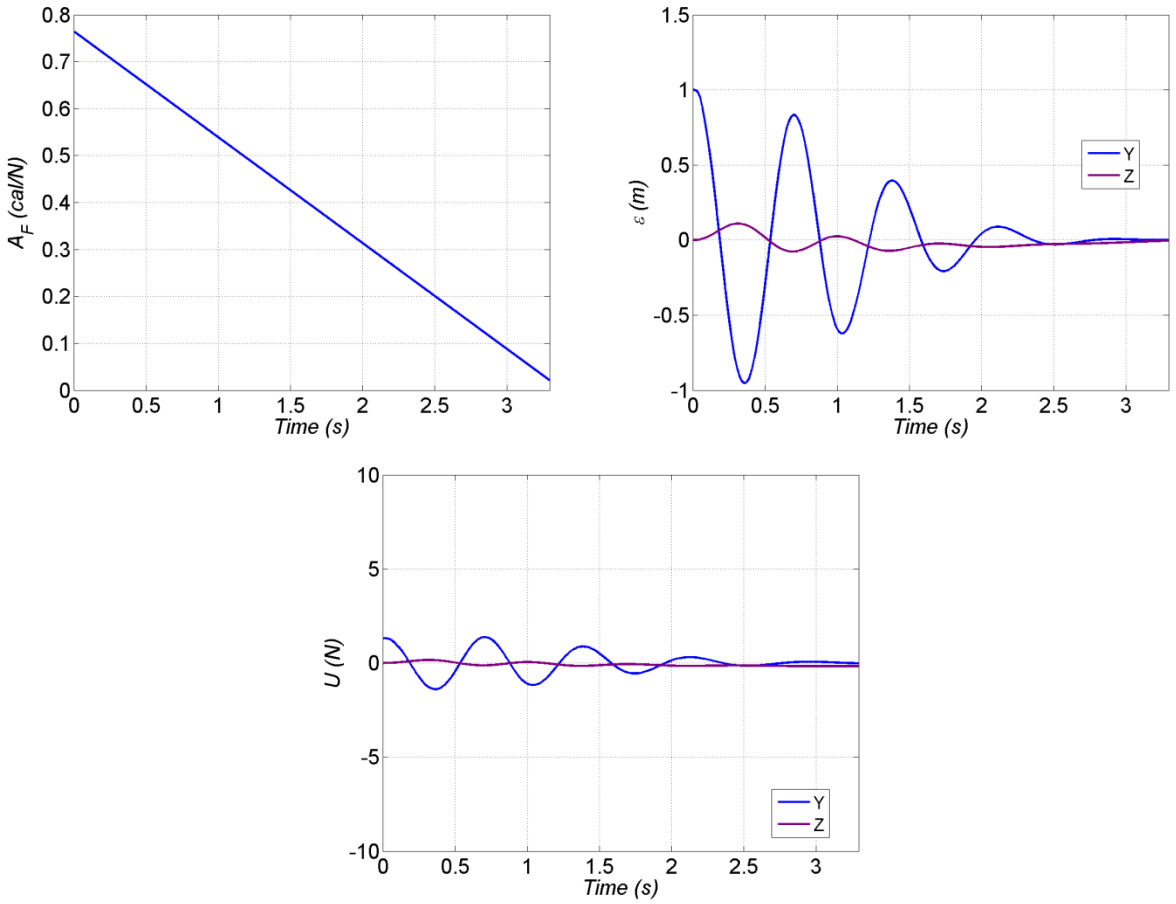

Fig. 6 Control metrics of parent and one child

The robustness of this control system to system error was addressed through Monte Carlo simulation. Variation or uncertainty in aerodynamics, mass properties, atmospheric, actuators, feedback measurements, and launch conditions were modeled as described previously. A sampling of Monte Carlo results for a parent and 2 children are given in Fig. 7–9 using a format similar to that in Fig. 4–6 for a parent and one child. The control goal for this situation is to fly the 2 children to impact 1 m to the left and right of the parent.

Figure 7 presents the flight-dynamic behaviors. Blue curves are for the parent, purple curves are for the first child, and now green curves are for the second child. The cross-range data in the

upper-left plot are interesting in that the parent flies off the line of fire, perhaps due to wind or errors in the feedback, and both children remain offset from the parent by 1 m to either side. The control metrics are also met in the vertical trajectory as the data for the parent and child bodies are very similar. This assessment has been conducted despite the difficulties associated with understanding the behavior of this modular-delivery concept (e.g., the need to simulate the instantaneous coupling of the bodies in flight with high fidelity). These trajectories indicate that the modular-delivery concept and guidance and flight-control laws are robust to system error.

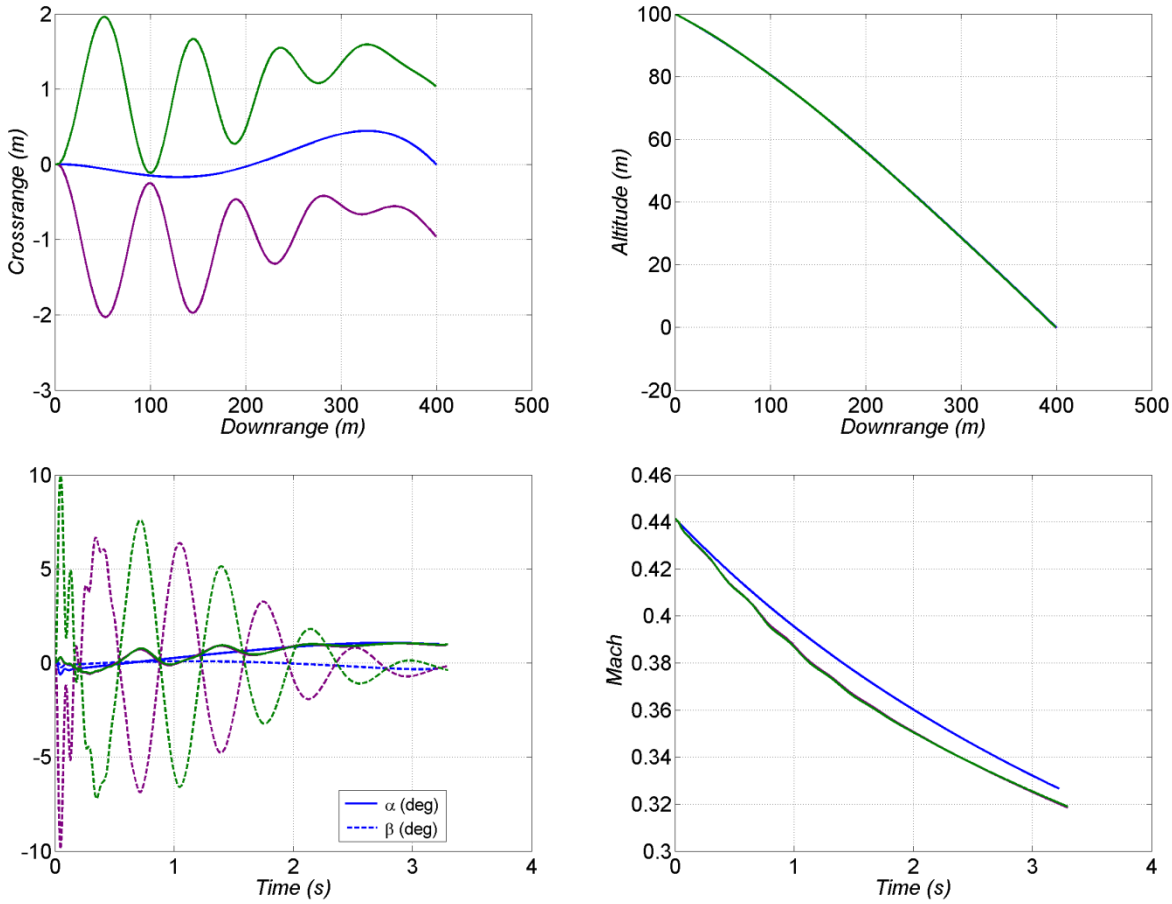

Fig. 7 Flight dynamics of parent and 2 children with uncertainty

The angle-of-attack (bottom-left) and Mach (bottom-right) histories in Fig. 7 are similar to those presented in Fig. 4. The yaw angle of attack for the 2 children is mirrored since one child flies on the left of the parent and the other is to the right. Mach number is similar for both children since the total angle of attack is similar.

The control input and output are given in Fig. 8 for a parent and 2 children with system uncertainty. Lateral-displacement feedback (left-most plot) is similar to that discussed in Fig. 5 except now the second-child data show up on the opposite side of the parent from the first child. The control commands are shown in the right-most plot just for the first child. These data closely

mimic data shown for the parent and one child. The only difference is due to the system errors considered in the present Monte Carlo result.

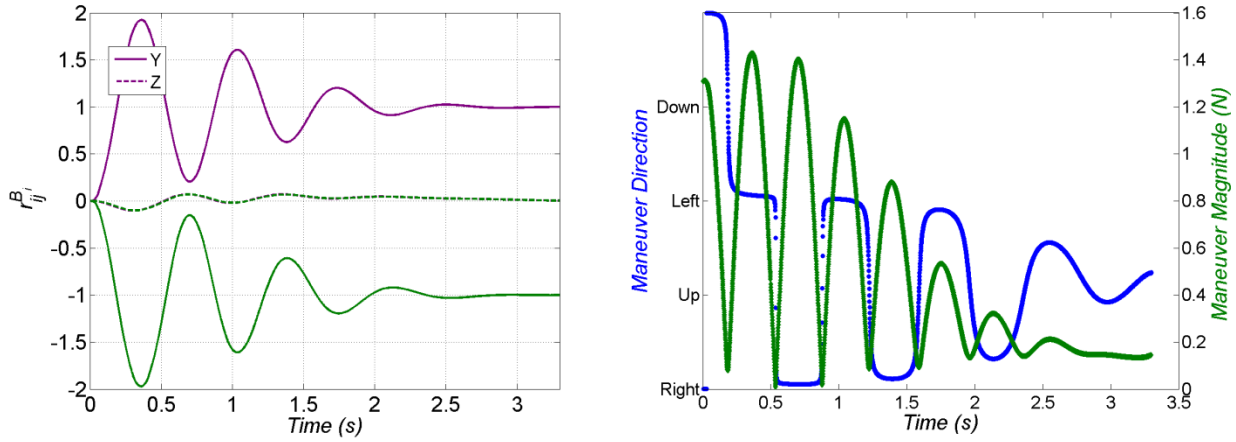

Fig. 8 Feedback output and control input of parent and 2 children with uncertainty

The control metrics of the control gain, control error, and control-force magnitude are shown in Fig. 9. Again, results are similar to those for the parent and one child. Control gain linearly decreases with time of flight. The errors and control forces decrease and oscillate with time. The majority of the control action is in the horizontal plane and the responses of the 2 children mirror each other.

The collective flight behavior of 10 bodies was investigated to assess the extensibility of the concept, guidance and flight-control algorithms, and simulations. One parent and 9 children were flown without uncertainty and with a desired pattern of 1-m radius from the parent with equal angular (i.e., 40°) increments. Format for presentation of these results follows that outlined previously.

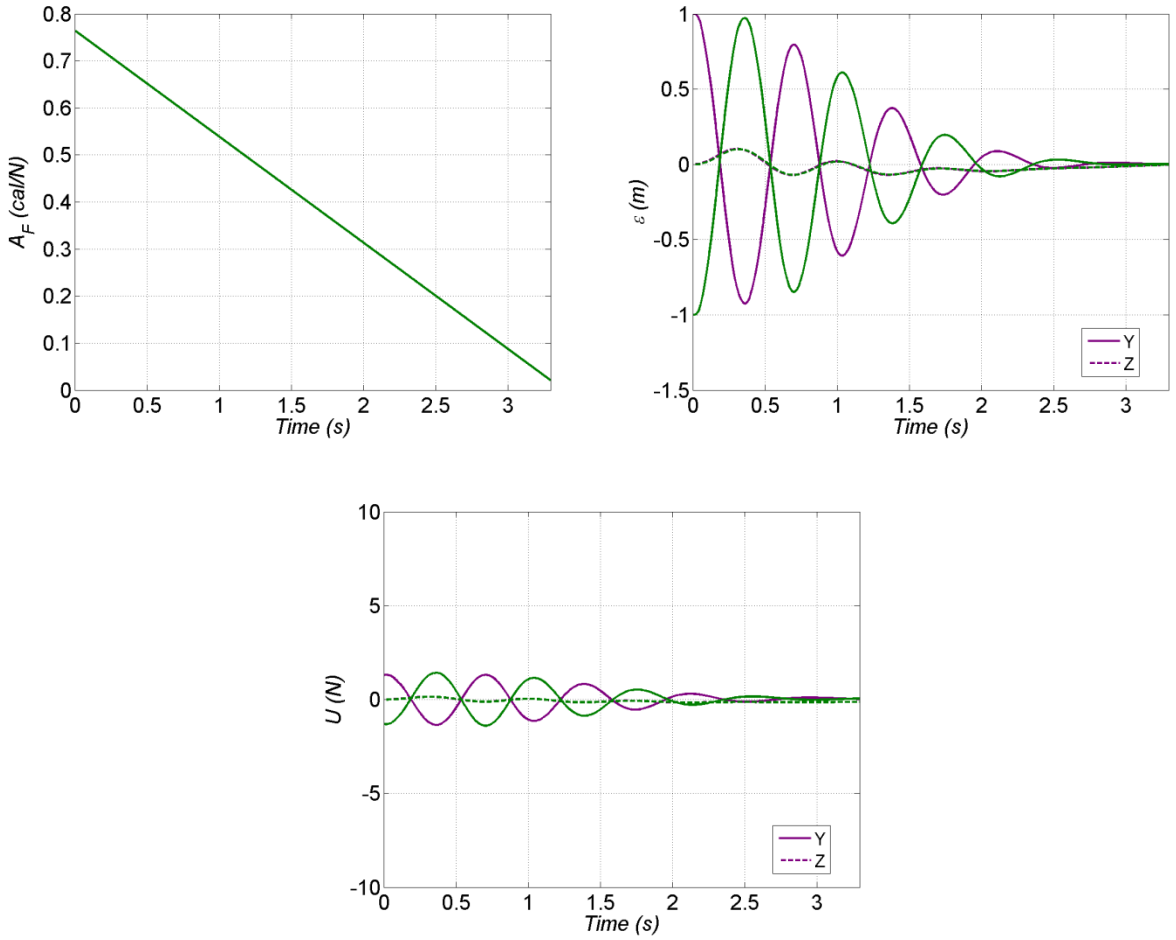

Fig. 9 Control metrics of parent and 2 children with uncertainty

Flight behaviors are collected in Fig. 10. A blue line denotes the parent and a variety of colored lines are for the 9 children. The trajectory results demonstrate excellent control performance as the swarm impacts at the target with the desired pattern. The cross-range and angle-of-attack data highlight the complexity associated with controlling the flight of multiple vehicles. Each child is steered through pitch and yaw angles of attack to yield a specific lateral displacement at impact (i.e., larger yaw angle of attack for larger desired cross-range impact).

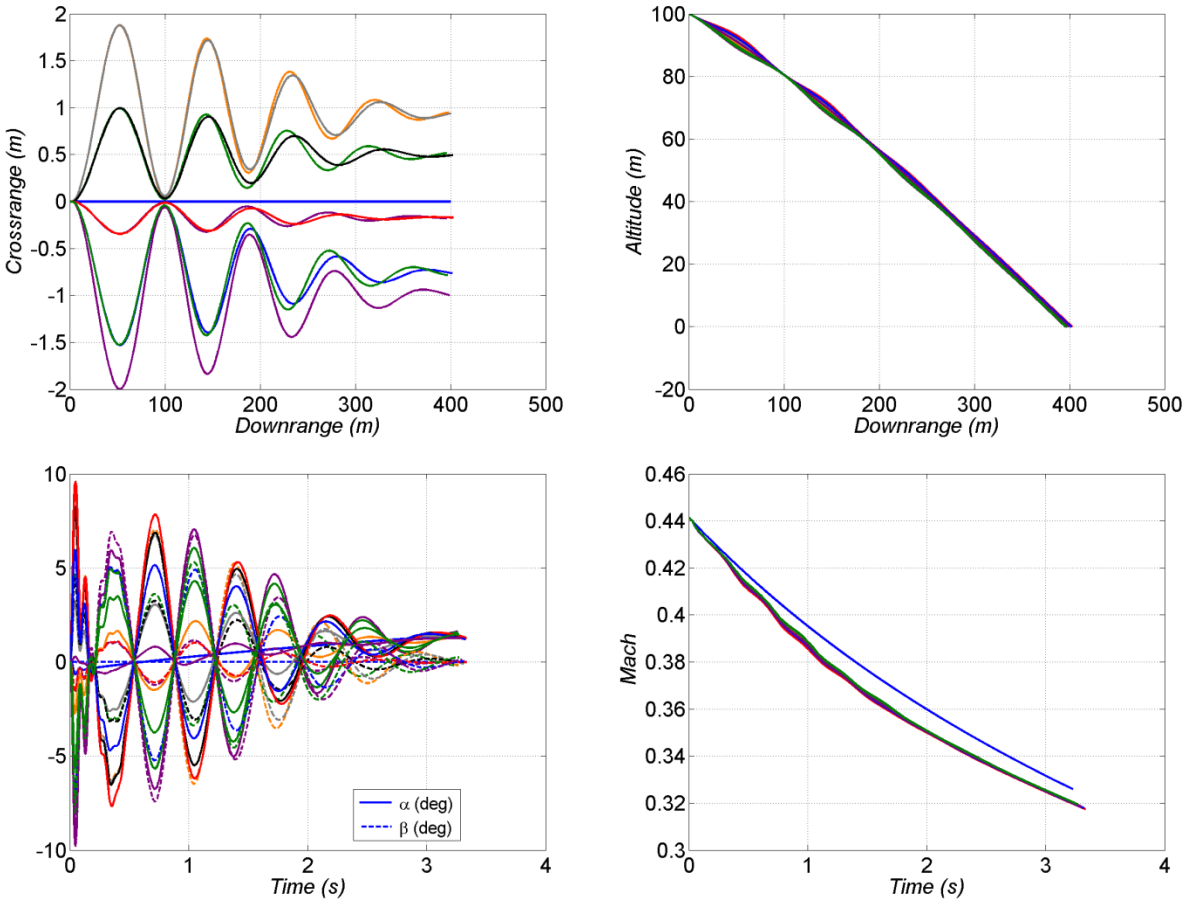

Fig. 10 Flight dynamics of parent and 9 children

The feedback in the left-most plot of Fig. 11 also demonstrates how the *y* and *z* components scale with the desired pattern. Some oscillation is evident in these data and the feedback for all 9 children stabilizes well to nearly a constant value for the latter half of the flights. The control commands for the first child, shown in the right-most plot of Fig. 11, replicate the data for a parent and one child in Fig. 5.

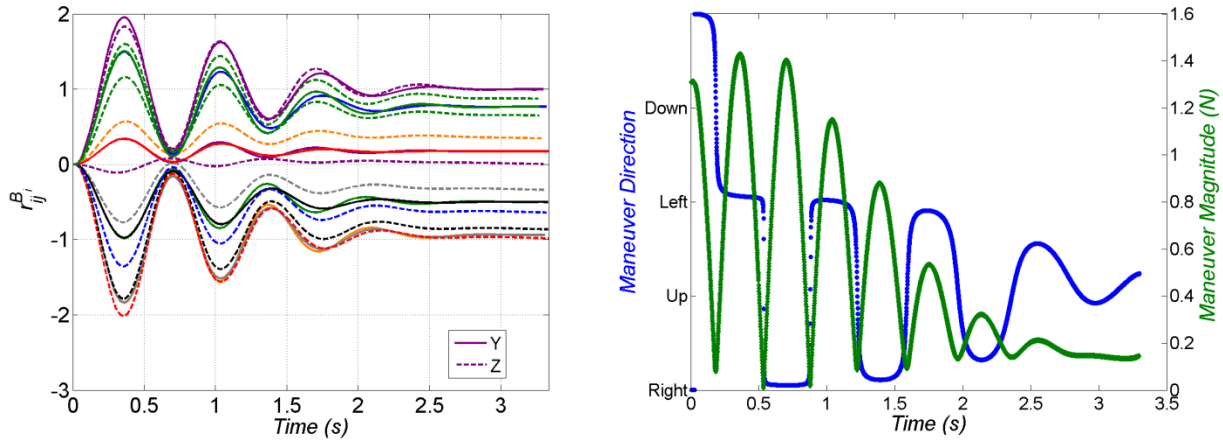

Fig. 11 Left, feedback output and control input of parent and 9 children; right, control commands for first child.

The control metrics are provided in Fig. 12 for completeness. Inspection of these data shows that the behavior of these data for 10 bodies follows the discussion in Fig. 6 and 9 for fewer bodies and with uncertainty.

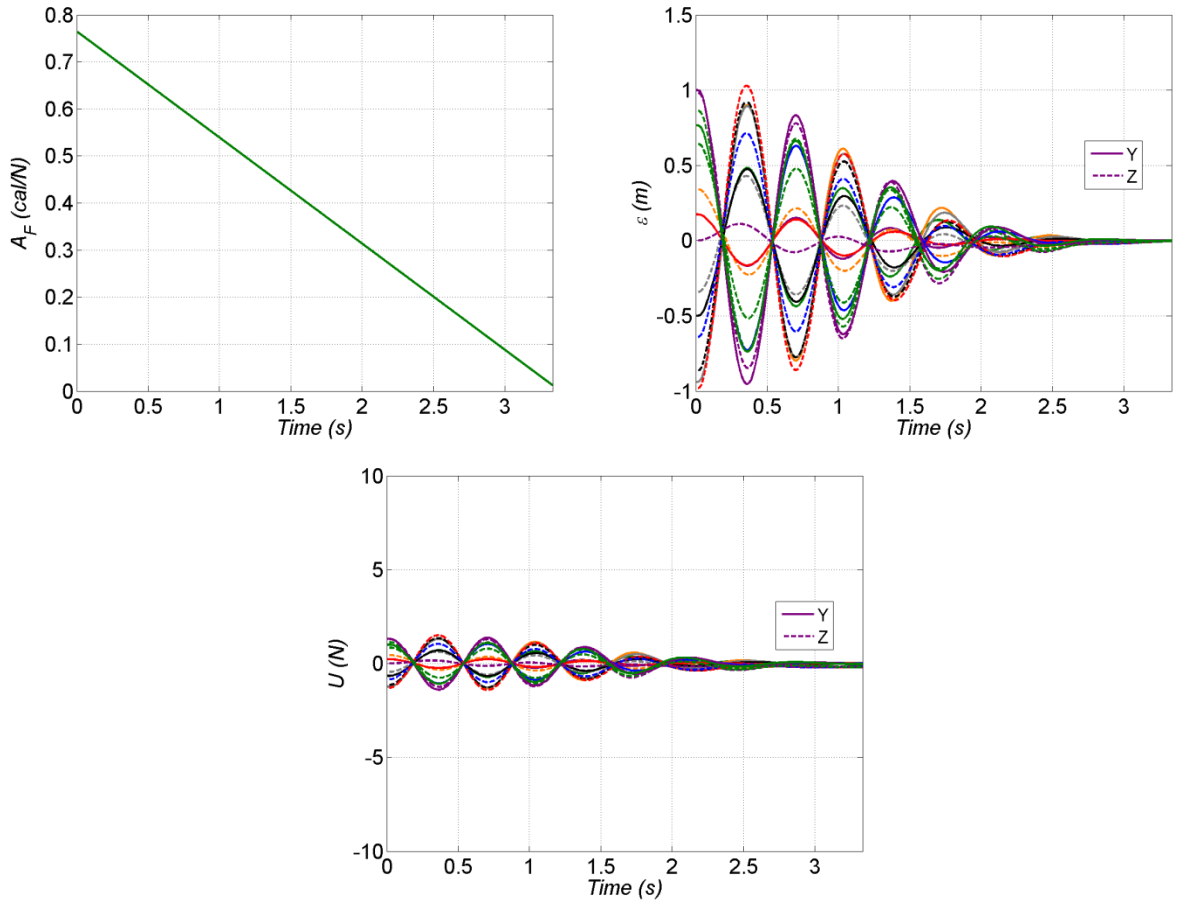

Fig. 12 Control metrics of parent and 9 children

6. Conclusions

Precision delivery of smaller, lethal modules on the battlefield for optimal efficiency could significantly enhance future weapon effectiveness. A major challenge to realizing this vision is the means of reliably achieving prescribed impact patterns without excessive cost. A parent–child concept, whereby a parent body possessing higher-performance components guides multiple child bodies equipped with simpler components to the target, was introduced.

Novel guidance and flight-control laws for this parent–child concept were derived. These algorithms were unique in using the flight dynamics to appropriately define the relationship between control input (thruster-force vector) and output (lateral displacement from other bodies) and optimization theory to resolve conflicts in formation flight for the child.

High-fidelity flight models were utilized to successfully demonstrate the concept and guidance and flight-control algorithms. Capturing nonlinearities in flight, feedback measurements, and control mechanisms was critical to proper assessment because this concept instantaneously couples the motions of multiple bodies in flight. Simulations (including Monte Carlo analysis) were challenging from a computing aspect but necessary to determine robustness to system uncertainties and extensibility to larger numbers of bodies flying to arbitrarily prescribed locations.

Results for a representative system demonstrated the feasibility of this concept. Despite the challenges of accommodating system nonlinearities with reduced feedback and simple thruster control, arbitrary delivery patterns were achieved even in the presence of uncertainties. The children flew at low total angle of attack (no evidence of flight instabilities) producing a slight decrease in Mach number from the parent. The lateral-displacement feedback from the ranging device was sufficient for control purposes. The control commands featured low force demands and reasonable directions. Varying control gains based on the flight dynamics was a major factor in the success of this concept. The control errors converged to zero. The means of reducing oscillation in the control errors and response include adding adjustable finite horizons or derivative terms to the controller.

7. References

1. Herbst WB. Future fighter technologies. J Aircr. 1980;17(8):561–566.
2. Nesline FW, Wells BH, Zarchan P. Combined optimal/classic approach to robust missile autopilot design. J Guid Cont Dyn. 1981;4(3):316–322.
3. Nesline FW, Zarchan P. Why modern controllers can go unstable in practice. J Guid Cont Dyn. 1984;7(4):495–500.
4. Wise KA, Broy DJ. Agile missile dynamics and control. J Guid Cont Dyn. 1998;21(3):441–449.
5. Kang S, Kim HJ, Lee J, Jun B, Tahk M. Roll-pitch-yaw integrated robust autopilot design for a high angle-of-attack missile. J Guid Cont Dyn. 2009;32(5):1622–1628.
6. Bennet DJ, McInnes CR, Suzuki M, Uchiyama K. Autonomous three-dimensional formation flight for a swarm of unmanned aerial vehicles. J Guid Cont Dyn. 2011;34(6):1899–1908.
7. Enright JJ, Savla K, Frazzoli E, Bullo F, Stochastic and dynamic routing problems for multiple uninhabited aerial vehicles. J Guid Cont Dyn. 2009;32(4):1152–1166.
8. Calise A, Preston D. Swarming/flocking and collision avoidance for mass airdrop of autonomous guided parafoils. J Guid Cont Dyn. 2008;31(4):1123–1132.
9. Ramirez-Riberos JL, Pavone M, Frazzoli E, Miller D. Distributed control of spacecraft formations via cyclic pursuit: theory and experiments. J Guid Cont Dyn. 2010;33(5):1655–1669.
10. Grubb ND, Belcher MW. Excalibur: new precision engagement asset in the warfight. Fires. 2008 Oct–Dec:14–15.
11. Fresconi FE. Guidance and control of a projectile with reduced sensor and actuator requirements. J Guid Cont Dyn. 2011;34(6):1757–1766.
12. Fresconi FE, Celmins I, Ilg M, Maley J. Projectile roll dynamics and control with a low-cost maneuver system. J Spacecr Roc. 2014;51(2):624–627.
13. Murphy CH. Free flight motion of symmetric missiles. Aberdeen Proving Ground (MD): Army Ballistic Research Laboratory (US); 1963 Jul. Report No.: BRL-TR-1216.
14. Fresconi FE, Celmins I, Silton S. Theory, guidance, and flight control for high maneuverability projectiles. Aberdeen Proving Ground (MD): Army Research Laboratory (US); 2014 Jan. Report No.: ARL-TR-6767. Also available at http://www.dtic.mil/dtic/tr/fulltext/u2/a593328.pdf

15. Silton S, Fresconi FE, Celmins I. High maneuverability airframe: investigation of fin and canard sizing for optimum maneuverability. Aberdeen Proving Ground (MD): Army Research Laboratory (US); 2014 September. Report No.: ARL-TR-7052.

16. Guidos B, Cooper G. Linearized motion of a fin-stabilized projectile subjected to a lateral impulse. J Spacecr Roc. 2002;39(3):384–391.

1 (PDF) DEFENSE TECHNICAL INFORMATION CTR DTIC OCA

2 (PDF) DIRECTOR US ARMY RESEARCH LAB RDRL CIO LL IMAL HRA MAIL & RECORDS MGMT

1 (PDF) GOVT PRINTG OFC A MALHOTRA

2 (PDF) ARO S STANTON M MUNSON

2 (PDF) VTD C KRONINGER B GLAZ

6 (PDF) RDECOM AMRDEC L AUMAN J DOYLE S DUNBAR B GRANTHAM M MCDANIEL C ROSEMA

1 (PDF) RDECOM ECBC D WEBER

41 (PDF) RDECOM ARDEC M BAKER G BISCHER D CARLUCCI J CHEUNG S K CHUNG D L CLER B DEFRANCO D DEMELLA M DUCA P FERLAZZO G FLEMING R FULLERTON R GORMAN R GRANITZKI N GRAY J C GRAU M HOHIL M HOLLIS R HOOKE W KOENIG A LICHTENBERG-SCANLAN S LONGO E LOGSDON M LUCIANO P MAGNOTTI G MALEJKO M MARSH G MINER J MURNANE M PALATHINGAL D PANHORST A PIZZA J ROMANO T RECCHIA G SCHLENK B SMITH C STOUT W TOLEDO E VAZQUEZ L VO C WILSON

2 (PDF) PEO AMMO C GRASSANO P MANZ

2 (PDF) PM CAS P BURKE M BURKE

1 (PDF) MCOE A WRIGHT

2 (PDF) ONR P CONOLLY D SIMONS

4 (PDF) NSWCDD L STEELMAN K PAMADI H MALIN J FRAYSSE

2 (PDF) NAWCWD P CROSS R SCHULTZ

2 (PDF) NAVAIR D FINDLAY J LEE T SHAFER

1 (PDF) AFOSR EOARD G ABATE

1 (PDF) MARCORSYSCOM P FREEMYERS

2 DARPA
(PDF) J DUNN
K MASSEY

1 NASA
(PDF) S VIKEN

1 DRAPER LAB
(PDF) G THOREN

1 GTRI
(PDF) A LOVAS

3 ISL
(PDF) C BERNER
S THEODOULIS
P WERNERT

2 DRDC
(PDF) D CORRIVEAU
N HAMEL

3 DSTL
(PDF) T BIRCH
R CHAPLIN
B SHOESMITH

3 DSTO
(PDF) S HENBEST
M GIACOBELLO
B WOODYAT

2 GEORGIA INST OF TECHLGY
(PDF) M COSTELLO
J ROGERS

1 ROSE-HULMAN INST OF TECHLGY
(PDF) B BURCHETT

1 AEROPREDICTION INC
(PDF) F MOORE

1 ARROW TECH
(PDF) W HATHAWAY

1 MARTEC LIMITED
(PDF) D ALLEXANDER

2 ATK
(PDF) R DOHRN
S OWENS

3 BAE
(PDF) B GOODELL
P JANKE
O QUORTRUP

GD OTS
D EDMONDS

UTAS
P FRANZ
S ROUEN
M WILSON

55 DIR USARL
(PDF) RDRL WM
P J BAKER
RDRL WML
M J ZOLTOSKI
P J PEREGINO
RDRL WML A
W OBERLE
M ARTHUR
R PEARSON
L STROHM
RDRL WML B
N J TRIVEDI
RDRL WML C
S A AUBERT
RDRL WML D
R A BEYER
A BRANT
J COLBURN
M NUSCA
Z WINGARD
RDRL WML E
P WEINACHT
V A BHAGWANDIN
I CELMIN
J DESPIRITO
L D FAIRFAX
F E FRESCONI
J M GARNER
B J GUIDOS
K R HEAVEY
R M KEPPINGER
G S OBERLIN
T PUCKETT
J SAHU
S I SILTON
RDRL WML F
M ILG
B ALLI
G BROWN
E BUKOWSKI
B S DAVIS
M DON
M HAMAOUI
K HUBBARD
B KLINE
J MALEY
C MILLER

P MULLER
B NELSON
B TOPPER
RDRL WML G
J T SOUTH
A ABRAHAMIAN
M BERMAN
M CHEN
W DRYSDALE
M MINNICINO
RDRL WML H
J F NEWILL
T EHLERS
M FERMEN-COKER
R PHILABAUM
R SUMMERS
RDRL WMM
J S ZABINSKI
RDRL WMP
D H LYON

INTENTIONALLY LEFT BLANK.